

## On the uniform approximation of the Reissner-Mindlin plate model by $p/hp$ finite element methods

**Christos Xenophontos\***

Department of Mathematical Sciences  
Loyola College, 4501 N. Charles Street, Baltimore, MD 21210, U.S.A  
e-mail: cxenophontos@loyola.edu

**Jason Kurtz and Scott R. Fulton**

Division of Mathematics and Computer Science  
Clarkson University, Potsdam, NY 13699, U.S.A.

**Key words:** Reissner-Mindlin plate,  $p/hp$  finite element method, shear locking, boundary layers

### **Abstract**

We study the approximation of the Reissner-Mindlin plate using the  $p/hp$  version of the finite element method (FEM). Our goal is to identify a method that: (i) is free of shear locking, (ii) approximates the boundary layer independently of the thickness of the plate and (iii) converges exponentially with respect to the number of degrees of freedom. We will consider both standard and reduced constraint/mixed formulations, in the context of the  $p/hp$  version of the FEM, and we will give guidelines for the construction of appropriate mesh-degree combinations that accomplish the above three goals, using straight as well as curved sided elements.

## 1 Introduction

The Reissner-Mindlin (R-M) plate model is a widely used system of partial differential equations, which describes the deformation of a thin plate subject to transverse loading. This two-dimensional model often replaces the full three-dimensional elasticity problem, when the thickness of the plate is small. To fix ideas, consider the bending of a homogeneous isotropic plate of thickness  $t > 0$ , occupying the region  $\mathfrak{R} = \Omega \times (-t/2, t/2)$ , where  $\Omega \subset \mathbb{R}^2$  represents the midplane of the plate, under normal load density per unit area given by  $gt^3$ . The equations of equilibrium for the *rotation*  $\vec{\phi} = (\phi_1, \phi_2)$ , and *transverse displacement*  $w$ , are

$$\begin{aligned} -\frac{D}{2} \left( (1-\nu)\Delta\vec{\phi} + (1+\nu)\nabla\nabla\cdot\vec{\phi} \right) - \kappa\mu t^{-2} (\nabla w - \vec{\phi}) &= 0 \\ \kappa\mu t^{-2} \nabla\cdot(\nabla w - \vec{\phi}) &= g \end{aligned} \tag{1}$$

where  $\nu$  is the Poisson ratio,  $\kappa$  is the shear correction factor,  $E$  is the Young's modulus and

$$D = \frac{E}{12(1-\nu^2)}, \mu = \frac{E}{2(1+\nu)}.$$

Multiplying the top equation in (1) by  $t^2$ , we see that the system is *singularly perturbed*. Hence, *boundary layers* will be present in the rotation (but not in the transverse displacement), as the thickness  $t$  tends to zero. Boundary layers, however, are not the only computational difficulty that one encounters when approximating the solution to the R-M plate model. As  $t \rightarrow 0$ , the solution  $u := (\vec{\phi}, w)$  tends to the limiting solution  $u_0 := (\vec{\phi}_0, w_0)$ , which satisfies *Kirchhoff's constraint*

$$\vec{\phi}_0 - \nabla w_0 = \vec{0}. \tag{2}$$

Practically, this means that the vertical fibers remain normal to the deformed midplane. The finite element solution must also satisfy a similar constraint and if the finite element space does not have enough functions satisfying (2), the approximate solution will be quite poor. This phenomenon is referred to as *shear locking* and conventional versions of the FEM can fail to overcome it. There are numerous papers aiming at designing “locking free” finite elements, (cf. [2] – [12] and the references therein), but only a handful address the use of high order  $p$  and  $hp$  versions of the FEM.

Our goal in this study is to address the question of how one can design a high order  $p/hp$  FEM that possesses three very important properties: (i) it is free of shear locking, (ii) it approximates the boundary layer independently of the thickness of the plate and (iii) it converges exponentially with respect to the number of degrees of freedom. In Section 2 we consider the above problem using the standard, as well as a mixed and a reduced constraint method, and in Section 3 we present the results of numerical computations for two benchmark problems. Our conclusions are summarized in Section 4. Throughout the paper, we will use the usual Sobolev space notation  $H^k(\Omega)$ , denoting the space of functions on  $\Omega$  with 0, 1, ...,  $k$  generalized derivatives belonging to the space of square integrable functions,  $L^2(\Omega)$ . The norm and seminorm on  $H^k(\Omega)$  will be denoted by  $\|\cdot\|_{k,\Omega}$  and  $|\cdot|_{k,\Omega}$ , respectively. Finally, the letter  $C$  will denote a generic positive constant independent of the thickness  $t$  and any discretization parameters.

## 2 The finite element methods

### 2.1 Standard formulation

The standard formulation of (1) reads: Find  $u_t := (\bar{\phi}_t, w_t) \in V = ([\Phi]^2 \times W) \subseteq [H^1(\Omega)]^2 \times H^1(\Omega)$  such that for all  $v := (\bar{\theta}, \zeta) \in V$

$$A_t(u_t, v) := a_t(\bar{\phi}_t, \bar{\theta}) + \kappa \mu t^{-2} \langle \nabla w_t - \bar{\phi}_t, \nabla \zeta - \bar{\theta} \rangle = \langle g, \zeta \rangle, \quad (3)$$

where  $\langle \cdot, \cdot \rangle$  denotes the usual  $L^2(\Omega)$  inner product and  $a_t(\cdot, \cdot)$  is given by

$$a_t(\bar{\phi}, \bar{\theta}) := \frac{D}{2} \int_{\Omega} \left\{ (1-\nu) [\nabla \phi_1 \cdot \nabla \theta_1 + \nabla \phi_2 \cdot \nabla \theta_2] + (1+\nu) (\nabla \cdot \bar{\phi}) (\nabla \cdot \bar{\theta}) \right\} dx_1 dx_2. \quad (4)$$

The space  $V$  above can be made more specific once boundary conditions are specified. For example, in the case of a *clamped* plate (i.e. zero Dirichlet conditions on the boundary  $\partial\Omega$ ),  $\Phi = W = H_0^1(\Omega)$ , where  $H_0^1(\Omega) = \{u \in H^1 : u|_{\partial\Omega} = 0\}$ , so that  $V = [H_0^1(\Omega)]^2 \times H_0^1(\Omega)$ .

The standard Galerkin finite element approximation of (3) proceeds by choosing a finite dimensional subspace  $V^N = ([\Phi^N]^2 \times W^N) \subset V$ , of dimension  $N$ , and seeking  $u_t^N := (\bar{\phi}_t^N, w_t^N) \in V^N$  such that

$$A_t(u_t^N, v) = \langle g, \zeta \rangle \quad \forall v = (\bar{\theta}, \zeta) \in V^N. \quad (5)$$

We then have

$$\|u_t - u_t^N\|_{E,\Omega} = \inf_{v \in V^N} \|u_t - v\|_{E,\Omega}, \quad (6)$$

where  $\|u\|_{E,\Omega} = (A_t(u, u))^{1/2}$  denotes the *energy* norm. It may be shown that there exist constants  $\alpha_1, \alpha_2 > 0$  such that

$$\alpha_1 \|u\|_{1,\Omega} \leq \|u\|_{E,\Omega} \leq \alpha_2 t^{-1} \|u\|_{1,\Omega}$$

hence, for fixed  $t > 0$ , the two norms are equivalent.

We mentioned above that as  $t \rightarrow 0$ , the solution  $u_t$  tends to  $u_0$ , which satisfies the constraint (2). The same constraint must be satisfied by  $u_t^N$ , in the limit, and if the space  $V^N$  does not have enough functions satisfying (2) the approximation will be quite poor. The finite dimensional subspaces  $V^N$  usually consist of piecewise polynomials on some subdivision (mesh) of the domain  $\Omega$ . The dimension  $N$  can be increased to improve accuracy by refining the mesh (*h* version), increasing the polynomial degree (*p* version) or both (*hp* version). In this study we will only consider the *p* and *hp* versions, which were shown to be asymptotically *free* of locking, at least when quasiuniform meshes consisting of straight-sided elements are used [12].

Due to the complicated nature of the interaction between the boundary layer and the locking effects, it is not completely clear how to precisely state a theorem that will describe the remedy and give bounds on the error. Instead, we will restrict ourselves to giving *guidelines* for the construction of the mesh-degree combination that will yield satisfactory (numerical) results. To accomplish this task, we use the results of [1] that describe the exact nature of the boundary layer, hence allowing us to construct appropriate mesh-degree combinations *a priori*. In particular, it was shown in [1] that under sufficient smoothness

on the loading function  $g$  and the boundary  $\partial\Omega$ , the solution  $u_t = (\bar{\phi}_t, w_t)$  of (3) satisfies

$$u_t = u_0 + t u_k^S + t u_k^{BL} + u_k^R \quad (7)$$

where  $u_0 = (\bar{\phi}_0, w_0)$  is the limiting solution satisfying (2),  $u_k^S = (\bar{\phi}_k^S, w_k^S)$  is the smooth part of the solution,  $u_k^{BL}$  is the boundary layer part of the solution, and  $u_k^R = (\bar{\phi}_k^R, w_k^R)$  is the smooth remainder.

All derivatives of  $\bar{\phi}_k^S, w_k^S, \bar{\phi}_k^R$  and  $w_k^R$  are uniformly bounded in  $t$ , and the boundary layer is given by

$$u_k^{BL} = (\chi \bar{\phi}_k^{BL}, 0) = \chi \sum_{i=1}^M t^i (\bar{\pi}_i(\rho/t, \theta) e^{-\sqrt{12\kappa}\rho/t}, 0) \quad (8)$$

where  $\chi$  is a smooth cut-off function,  $(\rho, \theta)$  are boundary fitted coordinates and  $\bar{\pi}_i(\rho, \theta)$  are polynomials in  $\rho$  with smooth in  $\theta$  coefficients (see [1] for more details). A key observation is that (8) shows that the boundary layer effect is essentially *one-dimensional*, namely in the direction normal to the boundary. (This can be seen from the presence of the term  $e^{-\sqrt{12\kappa}\rho/t}$ .) Using the above results, it was shown in [13] that if  $u_t^N = (\bar{\phi}_t^N, w_t^N)$  is the solution to (5), then

$$\|u_t - u_t^N\|_{E,\Omega} \leq C \left\{ \mathfrak{S}_0(w_0, N) + \mathfrak{S}_1(u_k^S, N) + \mathfrak{S}_2(\chi u_k^{BL}, N) + \mathfrak{S}_3(u_k^R, N) \right\} \quad (9)$$

where  $C > 0$  is a constant independent of  $t$  and  $N$ ,  $\mathfrak{S}_0(w_0, N) = \inf_{v_0 \in V^N} \|u_0 - v_0\|_{E,\Omega} \leq C \inf_{z \in W^N} \|w_0 - z\|_{2,\Omega}$ ,

$\mathfrak{S}_1(u_k^S, N) = \inf_{v \in V^N} \|u_k^S - v\|_{E,\Omega}$ ,  $\mathfrak{S}_2(\chi u_k^{BL}, N) = \inf_{\psi \in \Phi^N} \left\{ \|\chi u_k^{BL} - \psi\|_{E,\Omega} \right\}$  and  $\mathfrak{S}_3(u_k^R, N) = \inf_{z \in V^N} \|u_k^R - z\|_{E,\Omega}$ .

Since  $\mathfrak{S}_1$  represents the usual approximation rate of the space  $V^N$  and  $\mathfrak{S}_3$  is usually bounded by  $\mathfrak{S}_1$  for  $k$  large enough, the challenge lies in establishing  $\mathfrak{S}_0 \leq \mathfrak{S}_1$  and  $\mathfrak{S}_2 \leq \mathfrak{S}_1$ . If the first inequality holds then the method is *locking-free*. If the second inequality holds then the method *approximates boundary layers uniformly* in  $t$ . In order to construct a method that incorporates all the observations made thus far, we use the mesh-design principles from [14], in the context of the  $p/hp$  version of the FEM, in order to construct a finite element scheme with *robust* approximation properties. These guidelines suggest that one element of width  $O(pt)$ , where  $p$  is the polynomial degree of the approximating shape functions, along the boundary of the domain is sufficient to fully capture the boundary layer effects. The use of the  $p/hp$  version of the FEM, allows us to (at least) expect the method to be asymptotically free of locking [12] (even though our meshes will not be quasiuniform and/or our elements will have curved sides). We refer to [15] for a detailed study of what happens in the presence of curved elements in the pre-asymptotic range of  $p$ . The mesh-degree guidelines mentioned here will be made specific in Section 3 ahead when we consider the numerical solution of two benchmark problems.

## 2.2 Mixed methods

One alternative way to avoid locking (even when using the  $h$  version of the FEM) is to use a modified formulation, such a *mixed* or a *reduced constraint method*. In fact, these two approaches are, in some sense, equivalent. For a mixed method, the shear force

$$\bar{q} := [q_1(x, y), q_2(x, y)]^T = \kappa \mu t^{-2} (\nabla w - \bar{\phi}) \quad (10)$$

is introduced as an independent unknown and the following problem is solved: Find  $u_t = (\bar{\phi}_t, w_t) \in V$  and  $\bar{q}_t \in [L^2(\Omega)]^2$  such that

$$\begin{aligned}
 a(\bar{\phi}_t, \bar{\theta}) + (\bar{q}_t, \nabla \xi - \bar{\theta}) &= (g, \xi) \quad \forall v = (\bar{\theta}, \xi) \in V \\
 t^2 (\bar{q}_t, \bar{r}) - (\nabla w_t - \bar{\phi}_t, \bar{r}) &= 0 \quad \forall \bar{r} \in [L^2(\Omega)]^2.
 \end{aligned} \tag{11}$$

The discrete version arises by solving the above problem in finite dimensional subspaces  $V^N \subset V$  and  $Y^N \subset L^2(\Omega)$ , as usual. The ‘‘trade-off’’ is that now in order for the best approximation result (6) to hold, we must establish the so-called Babuška-Brezzi (inf-sup) condition for each pair of subspaces  $V^N$  and  $Y^N$  chosen (see e.g. [6]). This was done for a large class of such pairs corresponding to the  $h$  version of the FEM, and for certain pairs of subspaces corresponding to the  $hp$  version of the FEM (in the case of quasiuniform meshes with straight sided elements [11]). Recently, some work has been done towards the use of these methods with non-uniform mesh strategies [16], [17], but to our knowledge, there is no (theoretical) result that combines the necessary mesh design with mixed methods and gives error bounds showing the robustness (and possible exponential rates of convergence) expected with this approach.

### 2.3 Reduced constrained methods

An equivalent approach to mixed methods is, instead of introducing additional unknowns, to weaken Kirchhoff’s constraint. This is done via a *reduction operator*  $R_N : L^2(\Omega) \rightarrow S_N$ , where  $S_N$  is a space of polynomials, that satisfies

$$R_N(\nabla \xi) = \nabla \xi \quad \forall \xi \in W^N.$$

We then solve the following problem (instead of (5)): Find  $u_t^N := (\bar{\phi}_t^N, w_t^N) \in V^N$  such that

$$A_{t,N} := a_t(\bar{\phi}_t, \bar{\theta}) + \kappa \mu t^{-2} \langle R_N(\nabla w_t - \bar{\phi}_t), R_N(\nabla \zeta - \bar{\theta}) \rangle = \langle g, \zeta \rangle \quad \forall v = (\bar{\theta}, \zeta) \in V^N. \tag{12}$$

Note that by taking  $R_N \equiv I$ , we obtain the standard formulation (with  $A_{t,N}(u, v) = A_t(u, v)$ ), and if  $R_N \neq I$  we get a modified formulation. Various choices for  $R_N$  have been proposed in the literature (see [10] for an overview), varying from simple  $L^2$  projections to more sophisticated choices involving mixed interpolation [4]. For the analysis, one has to bound a *consistency* error, in addition to the usual approximation error:

$$\|u_t - u_t^N\|_{E,\Omega} \leq C \left\{ \inf_{v \in V^N} \|u - v\|_{E,\Omega} + \sup_{z = (\bar{\psi}, \zeta) \in V^N} \frac{|A_{t,N}(u, z) - (g, \zeta)|}{\|z\|_{E,\Omega}} \right\}. \tag{13}$$

For the calculation of the shear force, we then use

$$\bar{q}^N := \kappa \mu t^{-2} R_N(\nabla w_t^N - \bar{\phi}_t^N), \tag{14}$$

which corresponds to a (trivial) post-processing scheme for  $\bar{q}$ . See [10] for more details, including an alternative post-processing scheme for the shear. The mathematical analysis of  $p/hp$  reduced constraint methods is, to our knowledge, an open question.

## 3 Numerical results

In this section we present the results of numerical computations for two benchmark problems: a clamped rectangular plate and a soft simply supported circular plate. The domains and mesh design for these problems can be seen in Figure 1 below. Note the presence of *thin* elements of width  $pt$  along the boundary of each domain, where  $p$  is the degree of the approximating polynomial shape functions and  $t$

is the thickness of the plate. These “needle” elements are needed for the effective resolution of the boundary layer that is present in the solution [14]. Strictly speaking, in the case of the rectangular plate, we should also include *geometric refinement* near each corner, to accurately approximate the corner singularities that will arise (see e.g. [20]). In this problem, however, the singularities are not as severe as those that arise in, e.g. *L-shaped domains* [19], hence the boundary layer refinement will suffice. For both problems the polynomial degree was increased from  $p = 1$  to  $p = 7$ , uniformly over all elements in each mesh. Note that the location, and not the number of elements changes with  $p$ , hence this is not the “true” *hp* version, but rather the  $p$  version on a properly designed (moving) mesh. For all our computations, we will be interested in the (percentage) relative error in the energy norm

$$Error = 100 \times \frac{\|u_t^N - u_t\|_{E,\Omega}}{\|u_t\|_{E,\Omega}}, \quad (15)$$

as well as pointwise errors in the shear force (10), near  $\partial\Omega$ .

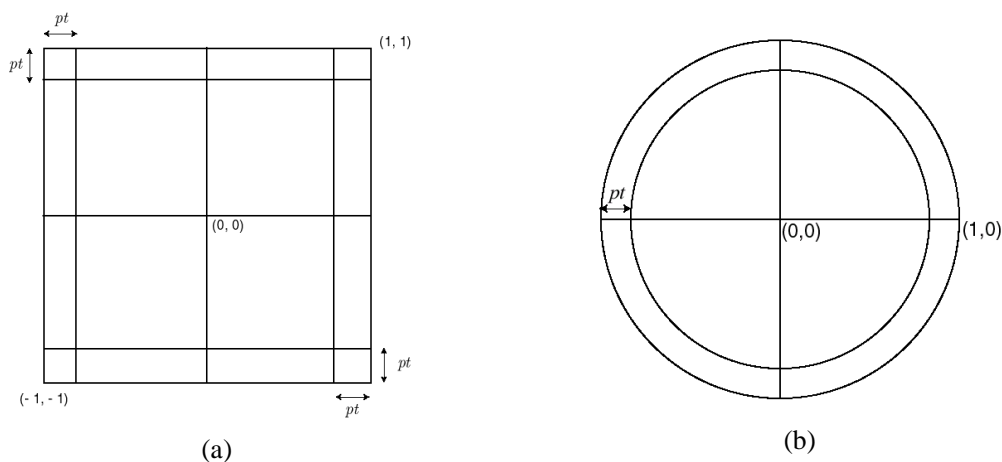


Figure 1: (a) Mesh for the rectangular plate. (b) Mesh for the circular plate.

### 3.1 Rectangular plate

We consider the case of a clamped rectangular plate with  $\Omega = [-1, 1] \times [-1, 1]$  (as seen in Figure 1(a)), loaded by  $g = 1$ , with Young's modulus  $E = 1$  and Poisson ratio  $\nu = 0.3$ . Figures 2 – 3 show the error, as given by (15), for various values of  $t$ , using the standard as well as the reduced constraint method. For the latter, we use the reduction operator  $R_N$  corresponding to the Raviart-Thomas spaces (see e.g. [11], [12]). As these figures show, the error appears to decrease at an exponential rate as  $p \rightarrow \infty$ , and both methods are robust when the error in the energy norm is of interest. For relatively large values of  $t$ , the reduced constrained method appears to perform slightly better. Figures 4 – 5 show the error in the pointwise shear force, near the boundary, for various values of  $t$ . In particular, we plot the first component of the shear  $q_1(x, 0)$ ,  $x \in (1 - t, 1)$ , as predicted by both methods using  $p = 7$ , along with a reference shear force obtained using a high(er) number of degrees of freedom. As these plots indicate, the standard method does not perform as well as it did in the energy norm, for small values of  $t$ , while the reduced constraint method maintained its robustness.

### 3.2 Circular plate

We next consider the case of a soft-simply-supported circular plate with  $\Omega$  being the unit disk (see

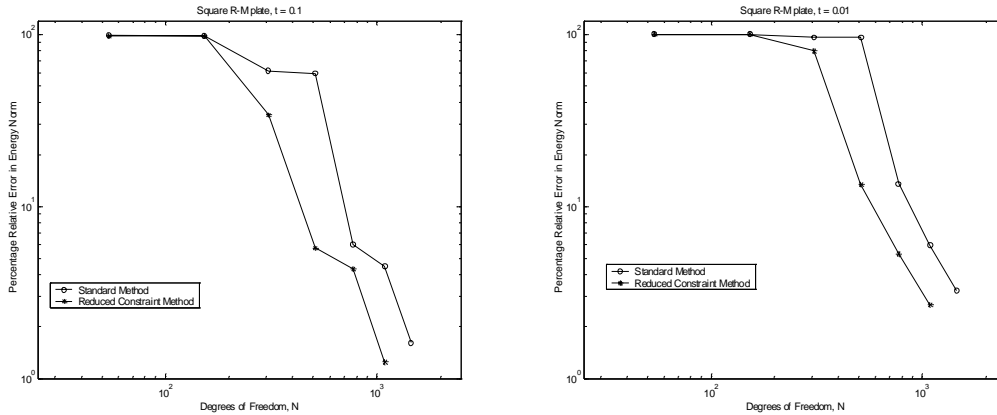


Figure 2: Convergence of the methods for the rectangular plate,  $t = 0.1, 0.01$ .

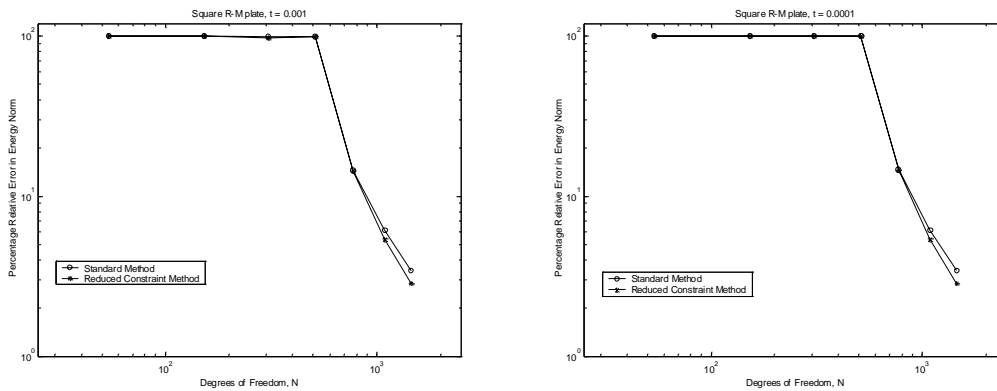


Figure 3: Convergence of the methods for the rectangular plate,  $t = 0.001, 0.0001$ .

Figure 1(b)), loaded by  $g$  given in polar coordinates by  $g(\vartheta) = \cos(\vartheta)$ , with Young's modulus and Poisson ratio as in the previous problem. An exact solution for this problem is readily available from [18]. Figures 6 – 7 show the error, as given by (15), for various values of  $t$ , as in the previous example. Both methods perform well, independently of  $t$ , and they seem to converge at an exponential rate. When the error in the shear force is computed, as seen in Figures 8 – 9, the performance of both methods seems to deteriorate as  $t \rightarrow 0$ , even though for relatively large values of  $t$  the results are rather satisfactory (with the reduced constrained method performing better than the standard one). This is (partially) due to the presence of curved elements (see [15], [17]). We are currently in the process of developing an alternative method (using a continuously differentiable approximation) that will hopefully alleviate this difficulty [17].

## 4 Conclusions

We have studied the finite element approximation of the solution to the Reissner-Mindlin plate model and the computational difficulties associated with it, namely the presence of shear locking and boundary layer effects. Our numerical results indicate that the  $p/hp$  version of the FEM performs very well, when

combined with the proper mesh-design principles. When the error in the energy norm is of interest, both the standard and the modified variational formulations produced satisfactory results and the error decreased at an (observed) exponential rate. When the error in the shear force was considered, the modified formulation performed noticeably better, especially when straight sided elements were used. In the presence of curved elements both methods deteriorated as  $t \rightarrow 0$ , and we are in the process of developing methods overcome this difficulty.

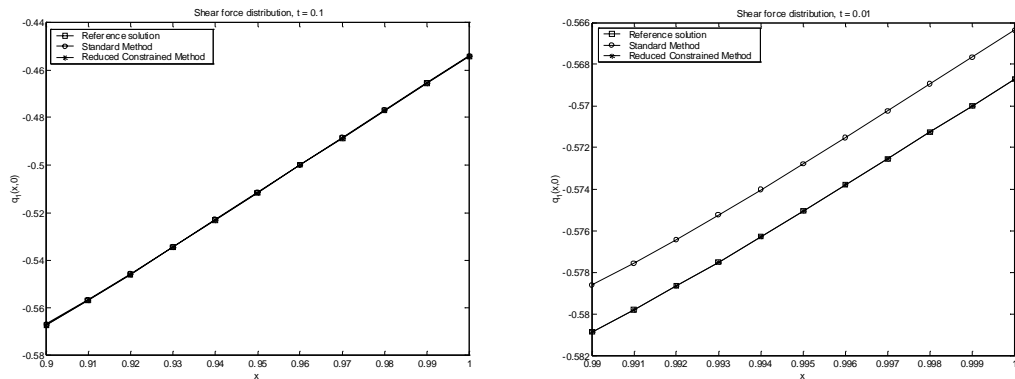


Figure 4: Shear force computation near the boundary for the rectangular plate,  $t = 0.1, 0.01$ .

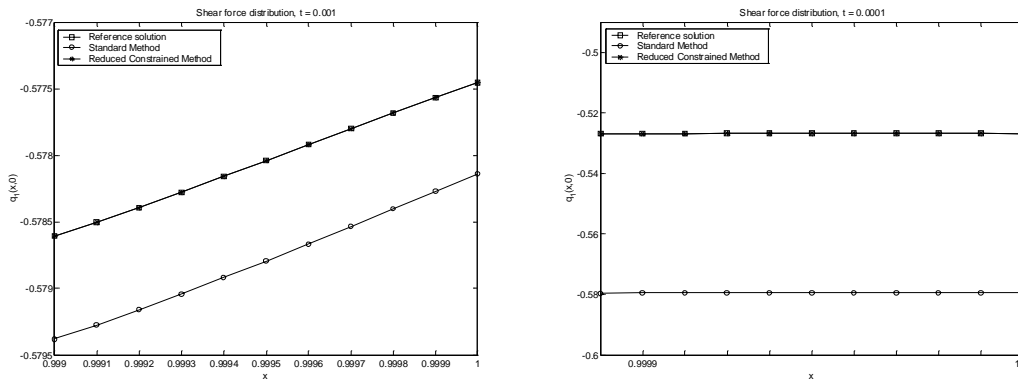


Figure 5: Shear force computation near the boundary for the rectangular plate,  $t = 0.001, 0.0001$ .

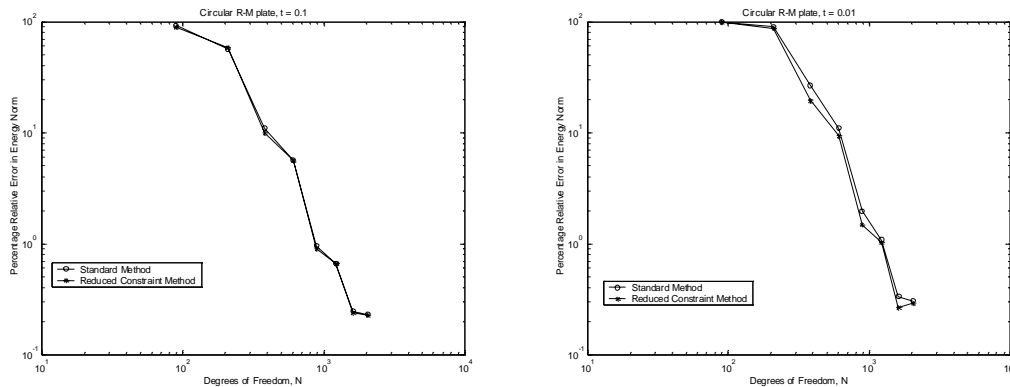


Figure 6: Convergence of the methods for the circular plate.

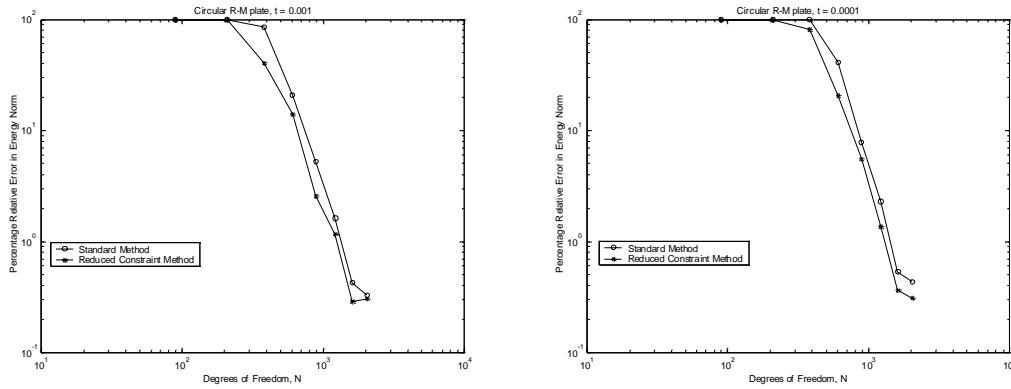


Figure 7: Convergence of the methods for the circular plate.

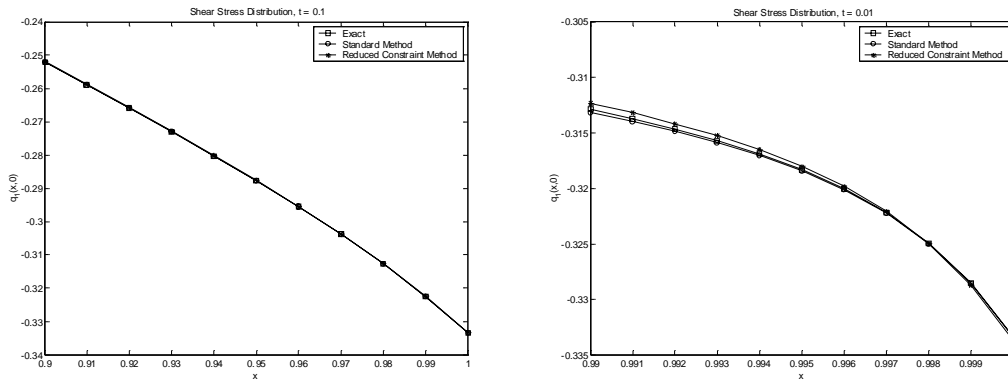


Figure 8: Shear force computation near the boundary for the circular plate,  $t = 0.1, 0.01$ .

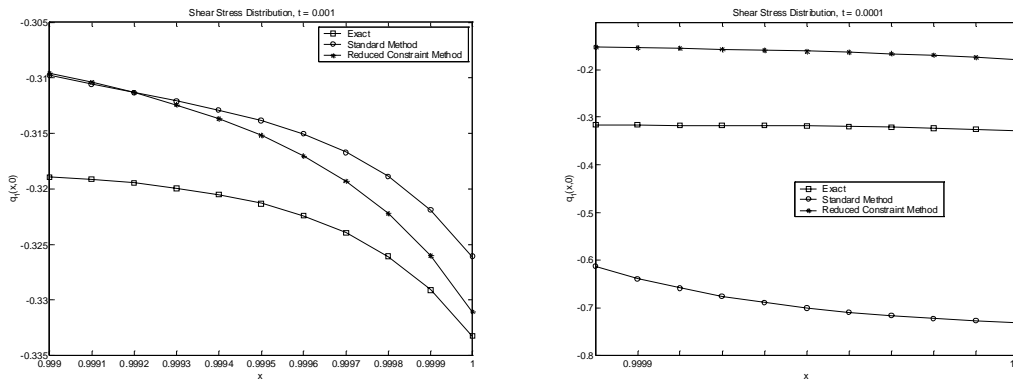


Figure 9: Shear force computation near the boundary for the circular plate,  $t = 0.001, 0.0001$ .

## References

- [1] Arnold, D. N. and Falk, R. S. (1996) “Asymptotic analysis of the boundary layer for the Reissner-Mindlin plate model”, *SIAM J. Math. Anal.*, Vol. 27, pp. 486 – 514.
- [2] Arnold, D. N. and Brezzi, F. (1989), “Innovative finite element methods for plates”, *Workshop on Innovative Finite Element Method, Rio De Janeiro, 27 November – 1 December*.
- [3] Arnold, D. N. and Falk, R. S. (1989) “A uniformly accurate finite element method for the Reissner-Mindlin plate”, *SIAM J. Num. Anal.*, Vol. 26, pp. 1276 – 1290.
- [4] Bathe, K. J., Brezzi, F. and Fortin, M. (1989) “Mixed interpolated elements for Reissner-Mindlin plates”, *Int. J. Numer. Meth. Eng.*, Vol. 28, pp. 1787 – 1801.
- [5] Brezzi, F. and Fortin, M. (1986) “Numerical approximation of Mindlin-Reissner plates”, *Math. Comp.*, Vol. 47, pp. 151 – 158.
- [6] Brezzi, F. and Fortin, M. (1991), *Mixed and Hybrid Finite Element Methods*, Springer-Verlag.
- [7] Brezzi, F., Fortin, M. and Stenberg, R. (1991), “Error analysis of mixed interpolated elements for Reissner-Mindlin plates”, *Math. Models and Methods in Applied Sciences*, Vol. 1, pp. 125 – 151.
- [8] Duran, R. and Liberman, L. (1992), “On mixed finite element methods for the Reissner-Mindlin plate model”, *Math. Comp.*, Vol. 58, pp. 561 – 573.
- [9] Hughes, T. J. R. and Franca, L. P. (1988), “A mixed finite element formulation for Reissner-Mindlin plate theory: Uniform convergence of all higher-order spaces”, *Comp. Meth. Appl. Mech. Eng.*, Vol. 67, pp. 223 – 240.
- [10] Pitkäranta, J. and Suri, M. (1996), “Design principles and error analysis for reduced-shear plate bending finite elements”, *Numer. Math.*, Vol. 75, pp. 223 – 266.
- [11] Stenberg, R. and Suri, M. (1997), “An  $hp$  error analysis of MITC plate elements”, *SIAM J. Numer. Anal.*, Vol. 34, pp. 544 – 568.
- [12] Suri, M., Babuška, I. and Schwab, Ch. (1995), “Locking effects in the finite element approximation of plate models”, *Math. Comp.*, Vol. 64, pp. 461 – 482.
- [13] Schwab, C. and Suri, M. (1994), “Locking and boundary layer effects in the finite element approximation of the Reissner-Mindlin plate model”, *Proc. Symp. Appl. Math.*, Vol. 48, pp. 367 – 371.
- [14] Schwab, C., Suri, M. and Xenophontos, C. (1997), “The  $hp$  finite element method for problems in mechanics with boundary layers”, *Comp. Meth. Appl. Mech. Eng.*, Vol. 57, pp. 311 – 334.
- [15] Kurtz, J. and Xenophontos, C. (2002), “On the effects of using curved elements in the approximation of the Reissner-Mindlin plate model by the  $p$  version of the finite element method”, submitted to *Applied Numerical Mathematics*.
- [16] Ainsworth, M. and Pinchedez, K. (2001), “The  $hp$ -MITC finite element method for the Reissner-Mindlin plate problem”, to appear in *J. Comp. Appl. Math.*
- [17] Kurtz, J. (2002), “On the uniform approximation of the Reissner-Mindlin plate model by the  $p/hp$  version of the finite element method”, M.S. Thesis, Division of Mathematics and Computer Science, Clarkson University, Potsdam, NY.
- [18] Arnold, D. N. and Falk, R. S., “Edge effects in the Reissner-Mindlin plate model”, *Analytical and Computational Models for Shells*, A.S.M.E., New York, 1989.
- [19] Xenophontos, C. (1998), “Finite Element computations for the Reissner-Mindlin plate model”, *Comm. Numer. Meth. Eng.*, Vol 14, pp. 1119 – 1131.
- [20] Szabó B. and Babuška I. (1991), *Finite Element Analysis*, John Wiley & Sons, Inc., New York.